

See discussions, stats, and author profiles for this publication at: <http://www.researchgate.net/publication/272374555>

Mechanical properties of milk protein SKIN layers after drying: Understanding the mechanisms of particle formation from whey protein isolate and native phosphocaseinate

ARTICLE *in* FOOD HYDROCOLLOIDS · FEBRUARY 2015

Impact Factor: 4.28 · DOI: 10.1016/j.foodhyd.2015.01.014

DOWNLOADS

65

VIEWS

76

7 AUTHORS, INCLUDING:



[Ludovic F Pauchard](#)

French National Centre for Scientific Resea...

53 PUBLICATIONS 740 CITATIONS

SEE PROFILE



[Cécile Le Floch-Fouéré](#)

Agrocampus Ouest

27 PUBLICATIONS 36 CITATIONS

SEE PROFILE

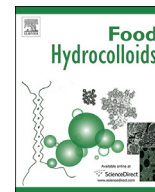


[Romain Jeantet](#)

Agrocampus Ouest

77 PUBLICATIONS 539 CITATIONS

SEE PROFILE



Mechanical properties of milk protein skin layers after drying: Understanding the mechanisms of particle formation from whey protein isolate and native phosphocaseinate



Céline Sadek^{a, b, c}, Ludovic Pauchard^d, Pierre Schuck^{b, c}, Yannick Fallourd^a, Nicolas Pradeau^a, Cécile Le Floch-Fouéré^{b, c, *}, Romain Jeantet^{b, c}

^a United Pharmaceuticals, F-75000 Paris, France

^b INRA, UMR1253, F-35000 Rennes, France

^c Agrocampus Ouest, UMR1253, F-35000 Rennes, France

^d CNRS, UMR7608, F-91405 Orsay, France

ARTICLE INFO

Article history:

Received 15 October 2014

Received in revised form

13 January 2015

Accepted 15 January 2015

Available online 7 February 2015

Keywords:

Mechanical properties

Milk proteins

Phase transition

Particle shape

Drying behaviour

ABSTRACT

The spray drying of milk proteins usually leads to dry particles of which the final shape can influence physical and functional properties of powders. The aim of this study was to understand the mechanisms of particle formation by considering the mechanical properties of materials making up the two main classes of milk proteins: whey proteins and casein micelles. The progressive solidification of the interface of the droplet during drying time was studied by high speed camera and fluorescence microscopy, in different experimental conditions. The mechanical properties of the final protein materials were then characterized by micro indentation testing. The drying dynamics of whey protein and casein micelle droplets showed different timescales and mechanical lengths, whatever the drying conditions and the droplet configurations, leading to typical mechanical instability at the surface i.e. buckling and fracture. The interface of casein micelles reached sol–gel transition earlier estimated at around 156 g.L^{-1} following by elastic and plastic regimes in which the shell distorted and buckled to form a final wrinkled particle. In contrast, the interface of whey proteins became elastic at only half the drying time estimated at around 414 g.L^{-1} , retaining a spherical shape, which finally fractured at the end of drying. The mechanical difference between the two plastic shells might be explained by the behaviour of proteins in jamming conditions. Analogous behaviour could be discussed between the casein micelles and soft and deformable colloids on the one hand, and between whey proteins and hard spheres on the other.

© 2015 Elsevier Ltd. All rights reserved.

1. Introduction

The evaporation of a droplet, whether free falling in the air, suspended from a thin filament, or deposited on a substrate, has been extensively studied in the past and is still a significant subject for scientific and industrial research (Sadek, Schuck, et al., 2014). The evaporation of solute dispersions involves important physico-chemical phenomena such as solute and solvent transport, adsorption and interactions between solutes and phase transitions. As the solutes concentrate at the interface during evaporation of

the water, important rheological changes occur within the droplet, inducing its progressive transition to a solid state with a specific particle structure (Pauchard & Allain, 2003b). Thus the final shape of the particle depends on the physicochemical properties of the matter and the drying parameters. However, understanding precisely how the final shape is formed and how it can be controlled still represent a challenge.

Indeed, the final shape of film formed from biological solutions and protein dispersions has recently become an area of interest for many applications. For medical diagnostic purposes, some researchers have focused on the final pattern of human fluids such as synovial fluid (Shabalin & Shatokhina, 2007), whole blood (Sobac & Brutin, 2014) and DNA (Dugas, Broutin, & Souteyrand, 2005). This has mainly consisted of studying the evaporation of defined proteins, particularly lysozyme and bovine serum albumin (BSA)

* Corresponding author. Agrocampus Ouest, UMR1253, F-35000 Rennes, France. Tel.: +33 (0) 2 23 48 59 26.

E-mail address: cecile.lefloch@agrocampus-ouest.fr (C. Le Floch-Fouéré).

(Accardo et al., 2010; Annarelli, Fornazero, Bert, & Colombani, 2001; Gorr, Zueger, & Barnard, 2012; Tarasevich & Pravoslavnova, 2007; Yakhno, 2008). Moreover, many studies have investigated the potential of proteins such as whey proteins and sodium caseinates to form delivery systems for probiotics and active substances in the pharmaceutical and food industries (Burgain, Gaiani, Cailliez-Grimal, Jeandel, & Scher, 2013; Hogan, McNamee, O'Riordan, & O'Sullivan, 2001; Sadeghi, Madadlou, & Yarmand, 2014; Serfert et al., 2013; Zhang & Zhong, 2013).

According to the literature available on spray drying, different proteins may result in various types of particle morphology (Ameri & Maa, 2006; Faldt & Bergenstahl, 1996; Kim, Chen, & Pearce, 2009). For example, Maa, Costantino, Nguyen, and Hsu (1997) reported distinct particle shapes (spherical, donut-like and wrinkled particles) after the drying of three model proteins (rhDNase, rhuMAbE25 and BSA, respectively). Sadek, Li, et al. (2014) previously focused on the spray drying of two main milk proteins, i.e. whey proteins and casein micelles. A specific monodispersed droplet spray drier (MDS) was used in order to produce identical droplets though the same drying trajectory inside the drier. Two different types of morphology were clearly identified under controlled spray drying conditions; dense, wrinkled particles for casein micelles and hollow, spherical particles for whey proteins.

Each of these distinct morphologies resulted in the occurrence of different types of surface instability during evaporation. Pauchard & Allain (2003c) studied such physical phenomena on single droplets of colloid and polymer dispersions. They reported that the first instability is due to the formation of a permeable solid skin at the surface which bends under the pressure of solvent evaporation. Then, according to the mechanical properties of the skin, a large number of deformations, including invagination or fracture instability, may occur and finally shape the dried particle. The mechanical skin responses may be strongly linked to the internal properties of the material such as its porosity, thickness, viscoelasticity and microstructure.

Therefore, the aim of this study was to evaluate:

- i) Are particular mechanical properties of a dry skin layer associated with specific protein nature?
- ii) Do these mechanical properties explain the occurrence of surface instability during evaporation?

In other words, the aim of this study is to know if the nature of the protein may lead to a skin layer whose physical properties condition the way that a droplet or the shell responds to mechanical stress induced by the evaporation process. In order to investigate these questions, experiments were conducted with distinct proteins, i.e. whey protein isolates (WPI) and native phosphocaseinates (NPC) to form the dried material. Understanding the drying behaviour of the two different protein materials should therefore provide key information to be able to predict the final structure of milk powders and thus control their physical properties.

2. Materials and methods

In the first part, the drying process of a droplet has been reported according to two different configurations, i.e. a single, pendant droplet and a confined droplet. In the second part, the mechanical properties of the skins of different milk proteins have been characterized in order to establish the elastic and plastic behaviours of the protein materials. These results are then discussed to understand the occurrence of droplet deformation during the drying process.

2.1. Materials

Experiments were conducted with distinct proteins, i.e. whey protein isolates and native phosphocaseinates. These are the two main classes of proteins in milk according to the ratio 20:80 (WPI: NPC). They are distinct in size and structure. Whey proteins have a rigid, compact globular structure with well defined folding of the polypeptide chain. They are mainly constituted of 70% β -lactoglobulin, often in dimer form (molecular mass 36.6 kDa), with 20% α -lactalbumin (molecular mass 14.2 kDa) (Walstra, Wouters, & Geurts, 2005). Native phosphocaseinates, also called casein micelles, represent a complex association of caseins (α_{s1} -, α_{s2} -, β - and κ -caseins), phosphate and calcium ions organized into micellar structures. The casein micelles are dynamic structures interacting with the soluble phase and highly hydrated as they contain around 3.7 g of water per gram of casein (de Kruif, 1998). They can be considered as natural and colloidal microgels with diameters ranging from 30 to 300 nm, and thus very different from whey proteins. The feed solutions were prepared from two milk protein powders, whey protein isolates and native phosphocaseinates, obtained from industrial sources and presenting protein content around 89 and 82% (w/w), respectively. The two solutions were reconstituted at 100 g.L⁻¹ protein in osmoted water at 50 °C with continuous stirring for two days at 20 °C to ensure full dissolution. The pH for WPI and NPC concentrates was in the range of 6.59 ± 0.16 at 25 °C. Particle size was measured by dynamic light scattering using a Zetasizer NanoZS apparatus (Malvern Instruments, Malvern, United Kingdom). The different sizes of proteins ranged from 8 to 30 nm and from 108 to 300 nm for WPI and NPC proteins, respectively.

2.2. Methods

2.2.1. Observation of single, pendant droplet

The drying process of a single, pendant droplet and its final particle shape were studied according to Sadek et al. (2013). A pendant droplet was deposited on a hydrophobic surface (providing a contact angle of the single droplet > 100°) and placed in a dry environment (Fig. 1a). The impact of matter on droplet deformation in a suspended system might be more noticeable than in a sessile droplet which is known to collapse with gravity and pressure gradient (Chen et al., 2012). The temperature was kept constant at 20 °C whereas relative humidity (RH) was decreased to 2% in the presence of excess zeolites, in order to ensure a constant drying stress. A sealed glass chamber was used to reduce atmospheric disturbance. The hydrophobic surface was designed to ensure a small contact area with the droplet, making it possible to maintain the spherical shape of the droplet in order to limit its impact on droplet dynamics during drying. The external shape of the droplet was recorded with a high-speed camera (Fastcam MC2 10,000 NB, Photron, United States) equipped with suitable lenses (Zoom 6000, Navitar, United States). A light (Phlox 100/100 LLUB, Stemmer imaging, France) illuminated the droplet from behind to produce a uniform background. Drying took around 10 min, and data were recorded automatically every 10 s. Images from the camera were analysed with ImageJ software (U.S. National Institutes of Health). The final particle shape was also observed by scanning electron microscopy (SEM, model 6301, JEOL, Germany) at 7 kV and 100× after coating with gold/palladium.

2.2.2. Observation of confined droplet

The principle of a confined droplet is to sandwich a droplet between two circular, parallel horizontal glass slides, as a thin liquid film with $h \ll r(t)$ and to allow it to evaporate in this confined system (Fig. 1b). This two dimensional (2D) configuration bypassed

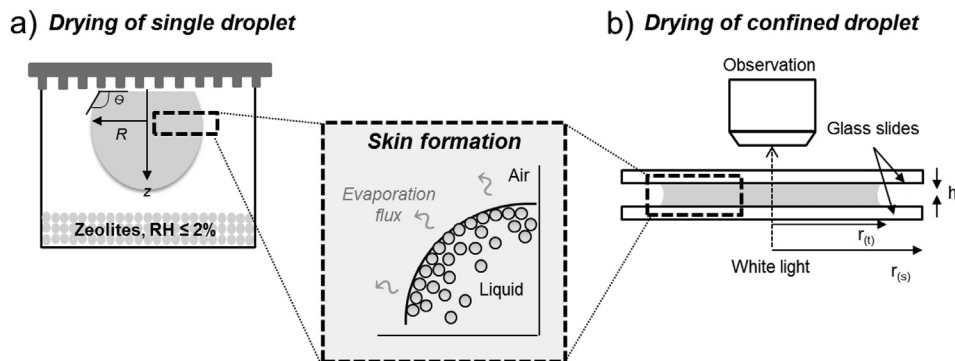


Fig. 1. Diagram of the two experimental setups: (a) single, pendant droplet and (b) confined droplet.

optical artefacts and permitted a more accurate observation of the local distribution of fluorescence which is not accessible in three dimensions (3D). The experiment was carried out according to a specific protocol explained in Boulogne, Giorgiutti-Dauphine, and Pauchard (2013). This confined system provides control of the water evaporation from the droplet meniscus toward the edge of the circular glass slides. Experiments were conducted at room temperature (20 °C) and 40% relative humidity. The proteins were labelled with fluorochrome rhodamine isothiocyanate (RITC, Sigma–Aldrich) by adding 20 μL of fluorescein solution (1 g L^{-1} RITC in dimethyl sulfoxide, DMSO, Sigma–Aldrich) to the 980 μL protein solutions before the experiment. RITC was excited at 570 nm, and the fluorescence from the solution was detected at 595 nm. Each droplet of 0.2 μL was squeezed between two glass slides of 16 mm in diameter with the distance between ensured by three 100 μm spacers. Placed at the periphery of the circular glass slides, these spacers did not affect the evaporation process or droplet deformation. Drying took around 60 min, and data were recorded automatically every 1 s. The evolution of the droplet edge and the fluorescence distribution within the droplet were observed using a fluorescent microscope (model BX51TF, Olympus, Japan) with light from a halogen lamp, a CDD camera (model QIClick, Qimaging, Canada) and a $\times 4$ magnification lens. Surface area and periphery length values were extracted from image analysis using Archimed (Microvision, France) and ImageJ computer software. The fluorescence profiles were measured for five other concentrations (25, 50, 80, 100, 200 g.L^{-1}) of WPI and NPC proteins in order to obtain the calibration curve (data not shown).

2.2.3. Indentation

A thin layer of WPI or NPC solution was deposited in a mould 5 mm in height and allowed to dry at room temperature 20 °C and relative humidity at 40%. The films were collected after the occurrence of fracture to be sure that the stress is released by fracture in the system. Moreover, during this step, we verified for each measurement that the indentation technique had not caused additional fractures in our samples. Indentation testing was then performed using an indentation tester (CSM, Anton Paar, Switzerland) with a spherical Rockwell indenter (Fig. 2a) in order to characterize the mechanical properties of the protein skins. The time-dependence of the stress release was investigated by creep measurements (Malzbender, Den Toonder, Balkenende, & de With, 2002): the indenter, initially in contact with the surface of the layer, was driven to the skin layer until a maximum of $F_0 = 50$ mN was reached, with a loading speed 50 mN min^{-1} (Fig. 2b). The maximum force was maintained during creep duration (here 1000 s).

Modelling the layer with a two-element Kelvin-Voigt model (a purely viscous damper and purely elastic spring connected in parallel as shown in Fig. 2c), and the time variation of the penetration depth h as a creep response to a constant external force F_0 could be expressed as:

$$p^{1.5}(t) = \frac{3}{4\sqrt{\alpha}} F_0 \left[\frac{1}{E} \left(1 - e^{-\frac{tE}{\eta}} \right) \right] \quad (1)$$

Eq. (1) was derived from the classic Hertz model during an elastic indentation of an infinitely stiff indenter in a sample with an elastic modulus E and a viscosity η , for a spherical indenter with a radius α .

A representative value of the skin layer yield stress, σ_y was estimated using the following semi-empirical relationship originally developed for metals (Tabor, 1951),

$$\sigma_y = \frac{F_0}{2.8A} \quad (2)$$

where the area of indentation, A , was the surface contact between the indenter and the skin layer. This was provided by $A = 24.5p_c^2 + 500.10^{-6}p_c$, where the contact depth, $p_c = p_{\text{max}} - \epsilon(F_0/S_{\text{max}})$ depends upon the maximum force applied F_0 , a geometric factor $\epsilon (=0.74)$, and the maximum slope of the unloading curve S_{max} (Fig. 7b) (Malzbender et al., 2002).

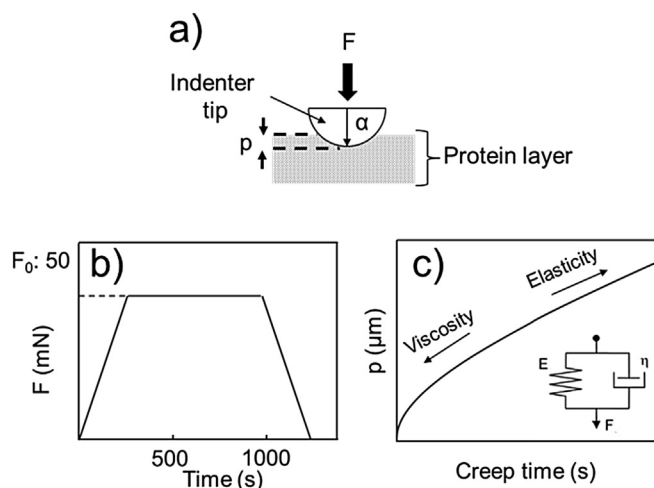


Fig. 2. Diagram of the indentation creep test method: (a) diagram of the spherical Rockwell indenter, (b) a typical load-time curve for the creep test and (c) typical creep curve consisting of a viscous state and an elastic state inserted into the linear viscoelastic creep (Kelvin-Voigt) model used to fit the experimental curves.

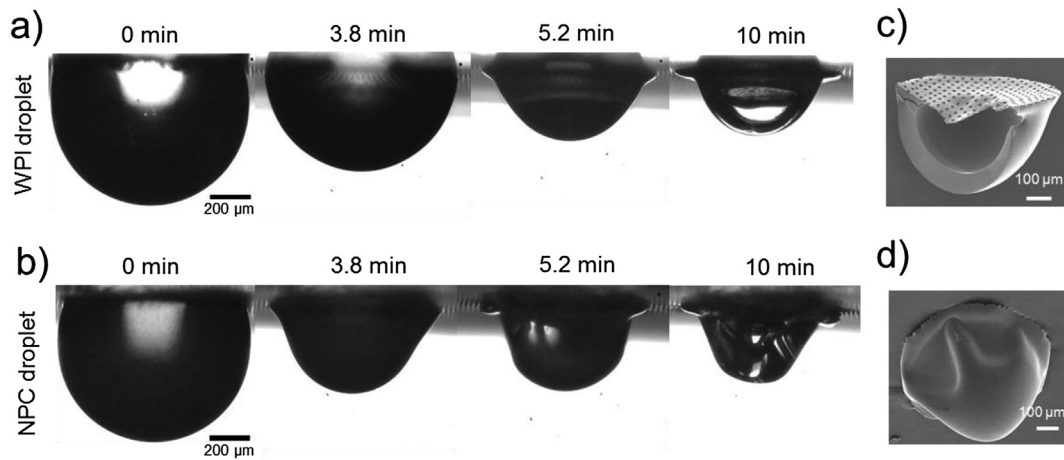


Fig. 3. Time lapse images of drying droplet profiles of (a) WPI droplet and (b) NPC droplet. SEM images (7 kV and 100 \times) of the fracture plane of the final dry WPI particle (c) and the entire dry NPC particle (d).

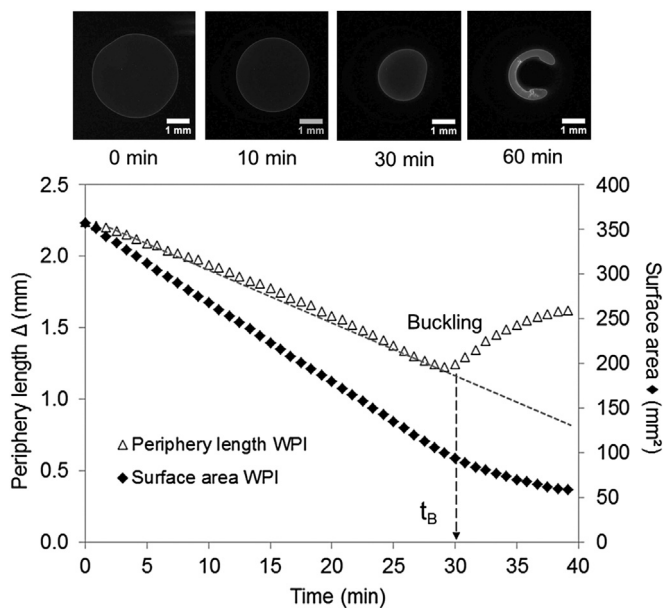


Fig. 4. Images of the confined whey protein isolate (WPI) droplet at different evaporation times (scale bar 1 mm). Graph: periphery length and surface area as a function of evaporation time.

Note that measurements of viscoelastic properties of materials using indentation testing do not yield absolute values but provide a process by which to compare the mechanical properties of different materials and characterization of the time evolution of the mechanical properties of the system.

3. Results and discussion

3.1. Drying dynamics of sessile droplets and particle shape

Two single, pendant droplets of WPI and NPC were first dried under the same stress conditions imposed by the lower relative humidity, in the presence of zeolites. Distinct and reproducible droplet deformation and particle shapes occurred between the two proteins (Fig. 3). Drying of the WPI droplet led to a smooth, semi-spherical particle shape (Fig. 3a, c). The particle was hollow and split into two parts at the end of drying (Fig. 3c). Drying of the NPC

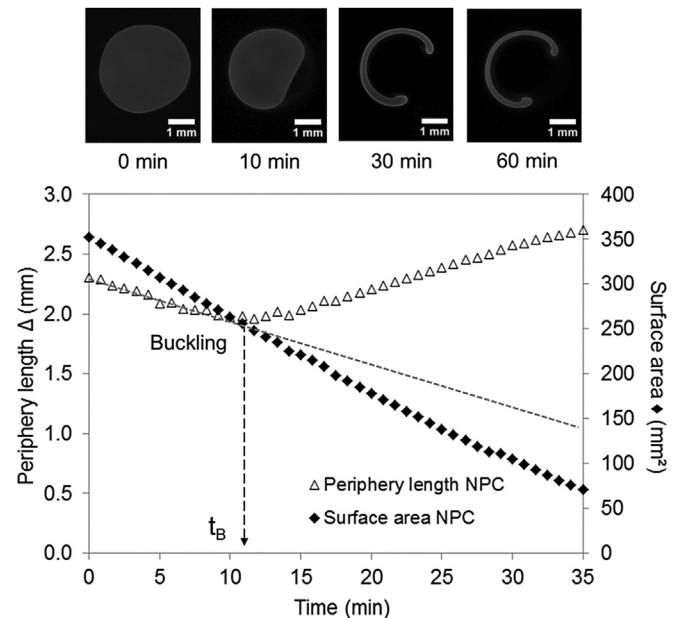


Fig. 5. Images of the confined whey protein isolate (NPC) droplet at different evaporation times (scale bar 1 mm). Graph: periphery length and surface area as a function of evaporation time.

droplet resulted in a twisted and wrinkled particle without any fractures (Fig. 3b, d).

Sadek et al. (2013) observed that the drying of a single WPI droplet comprised three distinct stages. At the beginning the water evaporated freely under diffusion controlled from the droplet surface towards the surrounding air. The droplet behaved as pure water, decreasing uniformly in volume and retaining its spherical shape. During the second stage, the evaporation process resulted in the accumulation of proteins at the interface, with distinct rheological properties between the surface and the droplet core. At this stage, shrinkage of the droplet slowed down and the formation of a gelled foot at the base revealed the occurrence of sol–gel transition at the surface. As a result, a skin progressively developed at the air–liquid interface, fixing the surface area of the droplet. Water evaporation was still possible through the porous skin. In the last stage, the skin thickened into a protein shell, leading to the formation of an internal vacuole. Finally, a random, single central

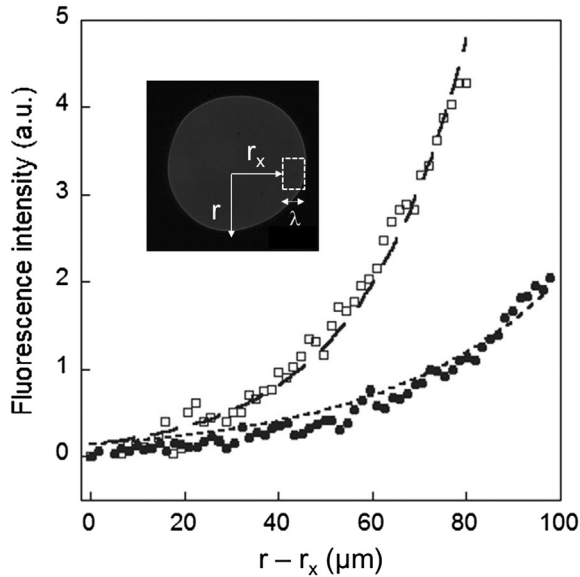


Fig. 6. Diffusion lengths (λ) of NPC proteins (\square) and WPI proteins (\bullet) measured at 500 s during the drying time.

fracture occurred at the end of drying that divided the droplet into two parts.

In this study, the same three stages were observed during the drying of a single droplet of NPC, but they were reached with different kinetics, and with different and specific deformations according to the type of protein (Table 1). The WPI droplet shrank over a longer time before the occurrence of buckling instability (around 5.2 min) whereas the NPC droplet rapidly became asymmetrical (before 3.8 min). The buckling of the NPC droplet occurred earlier in the drying process than that of the droplet of WPI, fixing a larger surface area. Once the skin was formed, the gelled droplets evolved in different ways during the last stage. Indeed, the NPC droplet was considerably distorted after buckling, revealing invaginations at the surface, whereas the WPI droplet remained spherical and did not evolve further, except in the interior where a large vacuole nucleated. This marked a clear difference between the drying dynamics of the NPC droplet and the WPI droplet. Wrinkles appeared throughout the last stage of NPC protein

Table 1

Comparison of the characteristic times and morphological features between the WPI droplet and NPC droplet.

Morphological features	WPI droplet	NPC droplet
$t_{buckling}$ (min)	5.2 ± 0.4	3.8 ± 0.0
$t_{invagination}$ (min)	—	5.1 ± 0.4
$t_{vacuole}$ (min)	7.5 ± 0.4	8.3 ± 0.0
Height/radius	0.56 ± 0.04	0.77 ± 0.07

drying, leading to a deflated particle shape with a small internal vacuole occurring at the end (Fig. 3d). In both cases, formation of the skin appeared to be necessary to obtain a vacuole (Arai & Doi, 2012), the nucleation of which strongly depended on the history of the droplet dynamics. The WPI vacuole filled the entire place inside the spherical, gelled droplet, whereas the vacuole occurred much later, after considerable distortion, and remained smaller for NPC.

Throughout the single, pendant droplet experiment, the two milk protein droplets showed distinct drying dynamics in terms of drying kinetics and droplet deformations. A direct impact on final particle shape occurred in accordance with that reported with the monodispersed droplet spray drier in a previous study (Sadek, Li, et al., 2014). The onset of buckling instability of colloidal suspensions was described with the theory of thin elastic shells (Pauchard & Allain, 2003a; Tsapis et al., 2005). Tsapis et al. (2005) reported that as water evaporated, the accumulation of colloids at the droplet surface induced the formation of a viscoelastic layer which became elastic, and then buckled. They suggested that forces between the colloids in the droplet may have an important role in determining the onset of buckling, and that capillary forces drive the deformation of the skin and overcome the electrostatic forces stabilizing the colloids against aggregation. However, in the study presented here, the two droplets distorted in different ways after the sol–gel transition, with invaginations for NPC and fracture of the spherical shell for WPI.

3.2. Dynamics of the interfaces of confined protein droplets

The temporal evolution of the surface area and the length of the periphery of the confined droplets of WPI and NPC proteins are presented in Figs. 4 and 5, respectively, showing two dynamic stages of the droplets during drying, whatever the protein material,

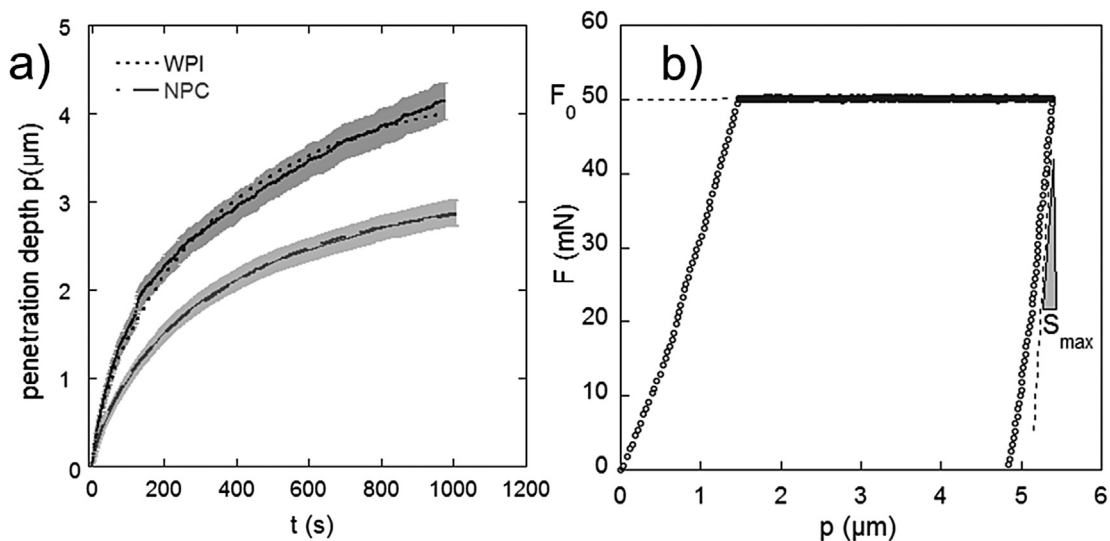


Fig. 7. Results of the indentation tests: (a) contact creep responses for WPI and NPC proteins, (b) representation of a load–displacement curve for WPI proteins.

i.e. isotropic shrinkage and then deformation by invagination. At the beginning, the confined droplets behaved as pure water by shrinking in a homogeneous way, as already observed by Giorgiutti-Dauphine and Pauchard (2013). As the water evaporated, the length of the periphery and the surface area of the confined droplet decreased keeping the circular shape. Then the sudden change in periphery length revealed an inversion of the curvature of the skin layer in both cases (Figs. 4 and 5). At this stage of drying, this local buckling instability resulted in a viscoelastic layer, as previously observed for the pendant droplet configuration. However, the increase in the length of the periphery indicated that the instability continued to progress inside the droplet. The local depression became deeper with time until a crescent-like shape was formed. Moreover, it appeared that the final shape resulted directly from the drying dynamics of the confined droplets. Fig. 4 shows a long stage of shrinkage for WPI before the occurrence of buckling instability at around 33 min (Table 2). The instability occurred on a small surface area, leading to a small pattern which finally fractured. In a similar way to the pendant droplet, the NPC proteins showed early distortions in the confined drying process. A local depression occurred from 11 min, whereas the convex part of the interface remained fixed. The invagination then progressed through a larger surface, leading to long, thin pattern.

Thus, whatever the droplet configurations (3D pendant droplet, 2D confined droplet, size), the device constraints (hydrophobic support, glass slides) and the drying conditions (relative humidity, temperature) making possible the occurrence of various hydrodynamic flows (Marangoni, Deegan and capillary flows) similar scenarios were observed for WPI and NPC proteins involving different kinetics to reach the surface instability. This suggests that the drying dynamics of the droplet might be more related to the instability of the system in terms of mechanical issues (induced by the development of an elastic skin) than in terms of hydrodynamic issues. These similarities between 2D and 3D configurations have already been reported for colloidal suspensions (Boulogne et al. 2013; Leng, 2010). Moreover, these authors observed a direct relationship between the initial volume fraction of colloids and the drying behaviour of the confined droplets. For example, Boulogne et al. (2013) reported that the duration of shrinkage increased when the initial volume fraction of colloids decreased. In addition, Leng (2010) described different final geometry of the material according to the nature of the dispersion. For large particles of polymethyl methacrylate (PMMA) with a radius of 3 μm they reported first a latency time during which the droplet remained circular, then the occurrence of a small depression and finally fracture of the skin. For the drying of smaller particles (PMMA particles, radius = 230 nm), they observed similar dynamics to the WPI droplet (i.e. a shrinkage stage) then buckling of the layer and the occurrence of a final fracture.

3.3. Gradients of protein concentration near the edge of the confined droplet

In a droplet, a radial flow is induced by the evaporation rate, V_E , that provides the typical velocity scale characterizing the transport of non-volatile components, such as proteins. A concentration profile is expected to develop on a typical length scale $\lambda = D_0/V_E$, this

ratio representing the gradient of proteins migrating towards the droplet–air interface as the water evaporates (Giorgiutti-Dauphine & Pauchard, 2013). The diffusion coefficient, D_0 , can be estimated using the Stokes–Einstein equation; $D_0 = k_B T / 6\pi\eta a$ leading to $D_{WPI} = 2.40 \times 10^{-11} \text{ m}^2 \cdot \text{s}^{-1}$ and $D_{NPC} = 2.08 \times 10^{-12} \text{ m}^2 \cdot \text{s}^{-1}$ as NPC and WPI proteins are significantly different in terms of size (Table 2). For each protein, the evaporation rate was estimated from image analysis of the size of the confined droplets at $V_E \sim 2 \cdot 10^{-7} \text{ m} \cdot \text{s}^{-1}$. The theoretical diffusion length (λ_{theo}) was estimated at 120 μm and 10 μm for WPI and NPC, respectively (Table 2). In addition, the diffusion length was estimated from the experiment, by measuring the fluorescence gradients near the droplet edge at 500 s, as shown in Fig. 6. The experimental values (λ_{meas} , Table 2) followed a similar trend with a shorter diffusion length for NPC proteins than for WPI proteins despite the different magnitude range. Note that the theoretical diffusion length does not take into account the drying time. Despite the fact that the measurements were made on the same time scale and with the same evaporation rate, the WPI and NPC droplets were not at the same drying stage at a given time. For example at 500 s, the NPC droplet was close to buckling whereas the WPI droplet was still shrinking. The difference observed in diffusion length therefore suggests that a lower NPC protein concentration is needed at the interface to induce a sol–gel transition than for WPI proteins, demonstrating that the latter, larger diffusion length is measured in droplet far from the buckling instability stage.

In order to confirm this hypothesis, evaluation of the critical concentration of proteins at the buckling time was approached by analysing the fluorescence profile of a confined droplet, which was expected to be proportional to the total amount of protein in the droplet while assuming that protein quantity is uniform in the vertical direction. The fluorescence intensity was measured just before the occurrence of buckling instability in the skin layer of the droplet, and converted into protein concentration through a calibration curve. The corresponding critical concentration was different according to the nature of the protein with $C_{buckling} = 156 \text{ g} \cdot \text{L}^{-1}$ for NPC and $C_{buckling} = 414 \text{ g} \cdot \text{L}^{-1}$ for WPI (Table 2). These results confirmed the differences in diffusion length between NPC and WPI in a way that suggested that NPC proteins may undergo a sol–gel transition at a lower critical concentration than WPI. Moreover, the concentration ranges were in accordance with previous studies focusing on the rheological behaviours and the phase transitions of proteins after concentration by an osmotic stress technique (Loveday, Creamer, Singh, & Rao, 2007). In particular, the rheological behaviour of concentrated β -lactoglobulin (which represents 70% w/w of WPI composition) was studied by oscillatory shear experiments (Parker, Noel, Brownsey, Laos, & Ring, 2005). The authors observed a solid-like response from $540 \text{ g} \cdot \text{L}^{-1}$, with a crossover of the storage modulus G' on the loss modulus G'' (frequency, $f \sim 2 \text{ Hz}$). This rheological transition was mainly influenced by the crowding of proteins which could no longer diffuse freely. Similar results were found for bovine serum albumin (which represents 5% w/w of WPI composition) with $G' > G''$ ($f \sim 1 \text{ Hz}$) for a concentration greater than $500 \text{ g} \cdot \text{L}^{-1}$ (Brownsey, Noel, Parker, & Ring, 2003). The authors predicted vitrification at a concentration higher than $600 \text{ g} \cdot \text{L}^{-1}$ for both whey proteins, leading to structure arrest. Casein micelles were similarly

Table 2
Characteristic values of the confined droplet dynamics and protein distributions during drying.

	Diameter (nm)	Time of buckling t_b (min)	Measured diffusion length λ_{meas} (μm)	Theoretical diffusion length λ_{theo} (μm)	Evaporation rate ($\text{m} \cdot \text{s}^{-1}$)	Concentration at $t_{buckling}$ ($\text{g} \cdot \text{L}^{-1}$)
WPI	18 \pm 17	33 \pm 4	37 \pm 0.3	120	2 $\cdot 10^{-7}$	414
NPC	208 \pm 97	11 \pm 2	23 \pm 0.1	10	2 $\cdot 10^{-7}$	156

analysed after osmotic stress concentration (Bouchoux et al., 2009; Dahbi, Alexander, Trappe, Dhont, & Schurtenberger, 2010). Bouchoux et al. (2009) reported that casein micelles showed elastic properties from 130 g.L^{-1} , with a significant increase in apparent viscosity. They interpreted these results as protein interactions through short-range repulsion produced by the κ -casein brush layer, present on the entire surface of the micelles. As the compression increases, the κ -casein layer may become flexible and the casein micelles may then come into contact and become close packed. A transition into a “soft solid” was estimated at around 178 g.L^{-1} with $G' > G''$ at low frequency ($f = 0.01 \text{ Hz}$). These results were confirmed by the work of Dahbi et al. (2010), who highlighted the beginning of an elastic regime from 148 g.L^{-1} where the apparent viscosity strongly increased and the occurrence of a solid state at around 170 g.L^{-1} according to oscillatory tests. Above 190 g.L^{-1} the system became dynamically arrested.

3.4. Mechanical properties of WPI and NPC skin layers

As the critical concentration approached, the surface of the droplet became elastic. At this stage the skin can withstand internal stresses through the onset of surface deformation. Deformation occurs mainly by bending, which is much less energy consuming than stretching (Boulogne et al., 2013). The protein skin layer was assumed to be homogeneous and characterized by an elastic modulus E , by a viscoelastic relaxation time-scale determined by the ratio η/E and a yield stress σ_y . The values for E , η , η/E and σ_y are given in Table 3 for WPI and NPC. In Fig. 7a, penetration in relation to time is represented for a constant load at 50 mN. It can be seen that the penetration depth was deeper for the WPI layer than for the NPC layer. The Kelvin-Voigt model (Eq. (1)) perfectly fitted the data and allowed estimation of the elastic modulus at 0.29 and 0.48 GPa for WPI and NPC, respectively. The values of the penetration depth and the elastic modulus thus suggest that the material made of the NPC proteins was stiffer than the WPI material at a given fracture time and peak load. Moreover, the viscoelastic relaxation time-scale was determined from the estimation of E and η , and revealed a higher value for NPC than WPI.

It is well known that the elastic modulus increases in the protein layer with time. The skin behaves as a coherent solid whose internal properties (thickness, microstructure) impede the free evaporation of water and lead to an increase in the drying stress as a function of time. When the drying stress reaches the skin layer yield stress, irreversible deformation caused by plasticity may occur. At this point, the structure is at arrest and macroscopic deformation such as the buckling process is then possible. In this study, the skin layer yield stresses were estimated through the load-displacement curve at 30 MPa for NPC and 52 MPa for WPI (Fig. 7b, Eq. (2)). With a lower value, the NPC material left the linear elastic regime earlier and reached plasticity well before the WPI material.

Although these indentation values cannot be considered real protein material parameters, due to their dependance on loading history (Chicot & Mercier, 2008), the mechanical properties of WPI and NPC materials can be compared and discussed in relation to our

previous results (pendant and confined droplets). A diagram of the possible skin formation mechanisms is proposed in Fig. 8.

As we saw, a gelled layer appeared sooner in the drying process of the NPC droplet ($t_{buckling} \sim 1/3 t_{drying}$) leading to the fixation of a larger surface area of the droplet. The elastic NPC skin rapidly reached the plastic stage, inducing the occurrence of early surface invaginations of the thin skin layer which behaved as a ductile plastic material (Fig. 8). On the other hand, the WPI droplet underwent a long shrinkage stage before buckling ($t_{buckling} \sim 1/2 t_{drying}$) in which the droplet greatly reduced in volume and was thus more concentrated at the interface. At buckling, the spherical elastic shell presented a smaller diameter. When the drying stress reached the yield stress of WPI, the shape remained identical but the occurrence of fracture reflected a brittle plastic material (Fig. 8).

The mechanical difference between the two plastic shells might be related to specific internal properties of the protein skin layers. In particular, the elastic modulus and the yield stress are known to depict the internal organization of the components of the material. Some researchers have described and discussed the rheological behaviour of globular proteins (β -lactoglobulin and bovine serum albumin) with viscosity models of hard sphere colloidal solid dispersion (Brownsey et al., 2003; Loveday et al., 2007; Parker et al., 2005). Despite the fact that aggregation of globular proteins involves specific binding sites, phase transitions may be understood by analogy with the behaviour of hard sphere dispersions revealing short range attractions and long range repulsions (Nicolai & Durand, 2007). In particular, it has been suggested that whey protein dispersions may be dominated by repulsive excluded volume interactions at high concentration values. As the volume fraction increased and the space available for particle motion decreased, the system became jammed. For hard spheres, the crowding of non-interacting particles led to a glasslike transition at volume fractions of about $\Phi = 0.58$. This solid state resulted from the permanent trapping of particles within cages formed by nearest neighbours (Pusey & van Meegen, 1986). The possible analogy between the rheological behaviour of WPI and undeformable hard sphere colloids could suggest a similar structural signature of the colloids. It is possible that as a hard sphere WPI might present similar intrinsic mechanical resistance under compression, inducing strong resistance to surface deformation, until reaching the yield stress where the shell fractures (Fig. 8) This behaviour is not expected for NPC as, in contrast to whey proteins, caseins are loose, self-assembled structures. Bouchoux, Gesan-Guiziou, Perez, and Cabane (2010) reported that the structure of the micelles is strongly affected by the rise in concentration. Above close packing, they reported that proteins continue to come into close contact and start to deform or deswell. The authors suggested a sponge-like model to describe the behaviour of casein micelles. Under compression, some soft regions of the micelle may lose water and collapse. The micelles finally merge with each other and form a continuous and irreversible material. Since it is known that caseins behave as hard spheres in dilute regimes, Dahbi et al. (2010) observed a strong deviation from the hard sphere model for higher concentrations (above $\sim 150 \text{ g.L}^{-1}$). However, the authors reported the same kind of rheological behaviour for casein micelles with a micro-gel model in jamming conditions. It therefore appears that casein micelles at high concentrations might be assimilated to soft deformable colloids such as foams and emulsions, as they are able to deform from the spherical shape and pack into specific disordered configurations (Douglas & Liu, 2001). In contrast to hard spheres, soft colloids can still hop around each other in a concentrated regime, allowing the skin deformation and thus explaining the ductile property of the plastic NPC material (Fig. 8).

Table 3
Estimated values and fit parameters of the creep curve as function of the load applied (50 mN).

	Viscosity, η (GPa.s)	Young's modulus, E (GPa)	η/E (s)	Yield stress, σ_y (MPa)
WPI	136 ± 0.6	0.29 ± 1.10^{-3}	469 ± 0.6	52
NPC	238 ± 0.3	0.48 ± 6.10^{-4}	496 ± 0.3	30

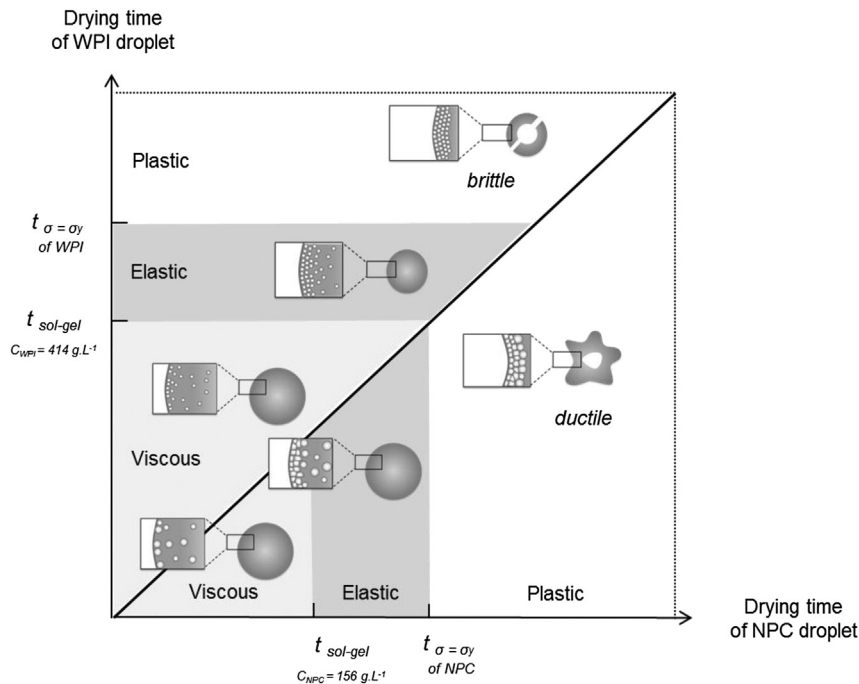


Fig. 8. Diagram of the different rheological regimes of skin formation of WPI and NPC droplets according to drying time.

4. Conclusion

Distinct and reproducible deformations were highlighted during the drying of single droplets of milk proteins. Whey proteins led to the formation of a smooth, spherical, broken particle whereas the casein micelles led to the formation of a twisted, wrinkled whole particle. These two milk proteins showed distinct drying behaviours in terms of drying kinetics and droplet dynamics, whatever the experimental conditions. The casein micelle layer rapidly reached the elastic regime ($t_{buckling} \sim 1/3 t_{drying}$) at a critical concentration estimated at around 156 g.L^{-1} whereas whey proteins became elastic after a long shrinkage stage ($t_{buckling} \sim 1/2 t_{drying}$) at a critical concentration of around 414 g.L^{-1} . After the sol–gel transition, the droplets underwent different types of surface instability (invaginations or fractures) which may be related to specific mechanical properties of protein materials. The way the proteins behave in jamming conditions may explain the network structure of the material and thus its mechanical properties. It is assumed that the brittle plastic characteristics of skin layer made of whey proteins may be explained by analogy with the concentration of non-interacting hard sphere colloids until crowding occurs where colloids are no longer able to flow and are caged between each other. At this point the system was arrested and fractured when the shear stress exceeded the yield stress. In contrast, the ductile elastic skin layer made of casein micelles was believed to result from the capacity of micelles to deswell as soft deformable spheres in jamming conditions. Their rearrangement allowed irreversible deformation of the shell leading to a wrinkled particle shape. Improved understanding of the physical phenomena taking place in jamming conditions may be of considerable importance for industry, especially in the control of spray drying. Indeed, prediction of the increase in viscosity and occurrence of phase transitions, and the understanding of the physical properties of the system should provide a powerful tool to control the structure of food. This study raises interesting questions such as whether the same mechanical properties would be found when using materials made of ideal systems such as hard spheres and microgels, and whether the

mechanical properties of the material can be managed by controlling the softness of the particle? These questions are the subject of ongoing investigations.

Acknowledgements

The authors thank United Pharmaceuticals for funding this work and for many fruitful discussions. We thank L. Joanny for the scanning electron microscopy observations.

References

- Accardo, A., Gentile, F., Mearini, F., De Angelis, F., Burghammer, M., Di Fabrizio, E., et al. (2010). In situ X-ray scattering studies of protein solution droplets drying on micro- and nanopatterned superhydrophobic PMMA surfaces. *Langmuir*, *26*, 15057–15064.
- Ameri, M., & Maa, Y. F. (2006). Spray drying of biopharmaceuticals: stability and process considerations. *Drying Technology*, *24*, 763–768.
- Annarelli, C. C., Fornazero, J., Bert, J., & Colombani, J. (2001). Cracks patterns in drying protein solution drops. *The European Physical Journal E*, *5*, 599–603.
- Arai, S., & Doi, M. (2012). Skin formation and bubble growth during drying process of polymer solution. *European Physical Journal E*, *35*, 1–9.
- Bouchoux, A., Debbou, B., Gesan-Guiziou, G., Famelart, M. H., Doublier, J. L., & Cabane, B. (2009). Rheology and phase behavior of dense casein micelle dispersions. *Journal of Chemical Physics*, *131*, 1–11.
- Bouchoux, A., Gesan-Guiziou, G., Perez, J., & Cabane, B. (2010). How to squeeze a sponge casein micelles under osmotic stress, a SAXS study. *Biophysical Journal*, *99*, 3754–3762.
- Boulogne, F., Giorgiutti-Dauphine, F., & Pauchard, L. (2013). The buckling and invagination process during consolidation of colloidal droplets. *Soft Matter*, *9*, 750–757.
- Brownsey, G. J., Noel, T. R., Parker, R., & Ring, S. G. (2003). The glass transition behavior of the globular protein bovine serum albumin. *Biophysical Journal*, *85*, 3943–3950.
- Burgain, J., Gaiani, C., Cailliez-Grimal, C., Jeandel, C., & Scher, J. (2013). Encapsulation of *Lactobacillus rhamnosus* GG in microparticles: Influence of casein to whey protein ratio on bacterial survival during digestion. *Innovative Food Science & Emerging Technologies*, *19*, 233–242.
- Chen, X. L., Boyko, V., Rieger, J., Reinhold, F., Reck, B., Perlich, J., et al. (2012). Buckling-induced structural transition during the drying of a polymeric latex droplet on a solid surface. *Soft Matter*, *8*, 12093–12098.
- Chicot, D., & Mercier, D. (2008). Improvement in depth-sensing indentation to calculate the universal hardness on the entire loading curve. *Mechanics of Materials*, *40*, 171–182.

- Dahbi, L., Alexander, M., Trappe, V., Dhont, J. K. G., & Schurtenberger, P. (2010). Rheology and structural arrest of casein suspensions. *Journal of Colloid and Interface Science*, 342, 564–570.
- Douglas, J. D., & Liu, A. J. (2001). Jamming in colloidal dispersions: hard sphere suspensions, emulsions and foams. In A. J. Liu, & S. R. Nagel (Eds.), *Jamming and rheology: Constrained dynamics on microscopic and macroscopic scales* (pp. 39–47). London: Taylor & Francis Ed.
- Dugas, V., Broutin, J., & Souteyrand, E. (2005). Droplet evaporation study applied to DNA chip manufacturing. *Langmuir*, 21, 9130–9136.
- Faltdt, P., & Bergenstahl, B. (1996). Spray-dried whey protein/lactose/soybean oil emulsions. 2. Redispersability, wettability and particle structure. *Food Hydrocolloids*, 10, 431–439.
- Giorgiutti-Dauphine, F., & Pauchard, L. (2013). Direct observation of concentration profiles induced by drying of a 2D colloidal dispersion drop. *Journal of Colloid and Interface Science*, 395, 263–268.
- Gorr, H. M., Zueger, J. M., & Barnard, J. A. (2012). Lysozyme pattern formation in evaporating drops. *Langmuir*, 28, 4039–4042.
- Hogan, S. A., McNamee, B. F., O'Riordan, E. D., & O'Sullivan, M. (2001). Emulsification and microencapsulation properties of sodium caseinate/carbohydrate blends. *International Dairy Journal*, 11, 137–144.
- Kim, E. H. J., Chen, X. D., & Pearce, D. (2009). Surface composition of industrial spray-dried milk powders. 2. Effects of spray drying conditions on the surface composition. *Journal of Food Engineering*, 94, 169–181.
- de Kruif, C. G. (1998). Supra-aggregates of casein micelles as a prelude to coagulation. *Journal of Dairy Science*, 81, 3019–3028.
- Leng, J. (2010). Drying of a colloidal suspension in confined geometry. *Physical Review E*, 82, 1–8.
- Loveday, S. M., Creamer, L. K., Singh, H., & Rao, M. A. (2007). Phase and rheological behavior of high-concentration colloidal hard-sphere and protein dispersions. *Journal of Food Science*, 72, 101–107.
- Maa, Y. F., Costantino, H. R., Nguyen, P. A., & Hsu, C. C. (1997). The effect of operating and formulation variables on the morphology of spray-dried protein particles. *Pharmaceutical Development and Technology*, 2, 213–223.
- Malzbender, J., Den Toonder, J. M. J., Balkenende, A. R., & de With, G. (2002). Measuring mechanical properties of coatings: a methodology applied to nanoparticle sol-gel coatings on glass. *Materials Science Engineering R*, 36, 47–103.
- Nicolai, T., & Durand, D. (2007). Protein aggregation and gel formation studied with scattering methods and computer simulations. *Current Opinion in Colloid & Interface Science*, 12, 23–28.
- Parker, R., Noel, T. R., Brownsey, G. J., Laos, K., & Ring, S. G. (2005). The nonequilibrium phase and glass transition behavior of β -lactoglobulin. *Biophysical Journal*, 89, 1227–1236.
- Pauchard, L., & Allain, C. (2003a). Buckling instability induced by polymer solution drying. *Europhysics Letters*, 62, 897–903.
- Pauchard, L., & Allain, C. (2003b). Stable and unstable surface evolution during the drying of a polymer solution drop. *Physical Review E*, 68, 1–4.
- Pauchard, L., & Allain, C. (2003c). Mechanical instability induced by complex liquid desiccation. *Comptes Rendus Physique*, 4, 231–239.
- Pusey, P. N., & van Meegen, W. (1986). Phase behaviour of concentrated suspensions of nearly hard colloidal spheres. *Nature*, 320, 340–342.
- Sadeghi, S., Madadlou, A., & Yarmand, M. (2014). Microemulsification-cold gelation of whey proteins for nanoencapsulation of date palm pit extract. *Food Hydrocolloids*, 35, 590–596.
- Sadek, C., Li, H., Schuck, P., Fallourd, Y., Pradeau, N., Le Floch-Fouéré, C., et al. (2014). To what extent do whey and casein micelle proteins influence the morphology and properties of the resulting powder? *Drying Technology*, 32, 1540–1551.
- Sadek, C., Schuck, P., Fallourd, Y., Pradeau, N., Le Floch-Fouéré, C., & Jeantet, R. (2014). Drying of a single droplet to investigate process – structure – function relationships: a review. *Dairy Science & Technology*, 1–24.
- Sadek, C., Tabuteau, H., Schuck, P., Fallourd, Y., Pradeau, N., Le Floch-Fouéré, C., et al. (2013). Shape, shell, and vacuole formation during the drying of a single concentrated whey protein droplet. *Langmuir*, 29, 15606–15613.
- Serfert, Y., Schröder, J., Mescher, A., Laackmann, J., Rätzke, K., Shaikh, M. Q., et al. (2013). Spray drying behaviour and functionality of emulsions with β -lactoglobulin/pectin interfacial complexes. *Food Hydrocolloids*, 31, 438–445.
- Shabalin, V. N., & Shatokhina, S. N. (2007). Diagnostic markers in the structures of human biological liquids. *Singapore Medical Journal*, 48, 440–446.
- Sobac, B., & Brutin, D. (2014). Desiccation of a sessile drop of blood: cracks, folds formation and delamination. *Colloids and Surfaces A: Physicochemical and Engineering Aspects*, 448, 34–44.
- Tabor, D. (1951). *Hardness of metals*. Oxford: Clarendon Press.
- Tarasevich, Y. Y., & Pravoslavnova, D. M. (2007). Segregation in desiccated sessile drops of biological fluids. *European Physical Journal E*, 22, 311–314.
- Tsapis, N., Dufresne, E. R., Sinha, S. S., Riera, C. S., Hutchinson, J. W., Mahadevan, L., et al. (2005). Onset of buckling in drying droplets of colloidal suspensions. *Physical Review Letters*, 94, 1–4.
- Walstra, P., Wouters, J. T. M., & Geurts, T. J. (2005). Milk components. Milk components. In P. Walstra, J. T. M. Wouters, & T. J. Geurts (Eds.), *Dairy science and technology* (2nd ed.). (pp. 76–79). London: Taylors & Francis Ed.
- Yakhno, T. (2008). Salt-induced protein phase transitions in drying drops. *Journal of Colloid and Interface Science*, 318, 225–230.
- Zhang, Y., & Zhong, Q. (2013). Encapsulation of bixin in sodium caseinate to deliver the colorant in transparent dispersions. *Food Hydrocolloids*, 33, 1–9.